CdTe Thin Films from Nanoparticle Precursors by Spray Deposition

Douglas L. Schulz,* Martin Pehnt, Doug H. Rose, Ed Urgiles, Andrew F. Cahill, David W. Niles, Kim M. Jones, Randy J. Ellingson, Calvin J. Curtis, and David S. Ginley

National Renewable Energy Laboratory, 1617 Cole Blvd., Golden, Colorado 80401-3393

The formation of CdTe thin films by spray deposition using nanoparticle colloids has been investigated. Employing a metathesis approach, cadmium iodide is reacted with sodium telluride in methanol solvent, resulting in the formation of soluble NaI and insoluble CdTe nanoparticles. After appropriate chemical workup, methanol-capped CdTe colloids were isolated. CdTe colloids prepared by this method exhibit a dependence of the nanoparticle diameter upon reaction temperature as determined by UV−visible spectroscopy (UV−vis), X-ray diffraction (XRD), and transmission electron microscopy (TEM). CdTe thin-film formation was performed by spray depositing the 25−75 Å diameter nanoparticle colloids according to a one- or two-step method. Films derived from a one-step approach were sprayed onto substrates at elevated temperatures ($T_{dep} = 280-440$ °C) with no further thermal treatment. Two-step films were sprayed at lower temperatures ($T_{dep} = 25-125$ °C) and were subjected to subsequent thermal treatments ($T_{anneal} = 250-500$ °C) in argon or forming gas (10% H_2 in N_2) ambients. The effects of a $CdCl_2$ treatment were also investigated for CdTe films on both 7059 glass and CdS on SnO_2-coated 7059 glass. The CdTe films were characterized by XRD, X-ray photoelectron spectroscopy (XPS), and atomic force microscopy (AFM). Phase-pure cubic CdTe formation was observed by XRD for two-step derived films (400 °C in forming gas) while one-step films were composed of the cubic CdTe and an oxide phase. XPS analysis of five films processed at 400 °C and a variety of conditions showed that while CdTe films produced by the one-step method contained no Na or C and substantial O, two-step films subjected to a $CdCl_2$ treatment showed reduced O but increased C content. AFM gave CdTe grain sizes of ~0.1−0.3 and ~0.3−0.7 μm for a one-step film sprayed at 400 °C and a two-step film annealed at 400 °C, respectively. The potential of employing CdTe nanoparticles toward photovoltaic technologies is discussed.

Introduction

Polycrystalline CdTe materials represent one of a few thin-film photovoltaic technologies presently being investigated by industry for terrestrial solar cell application. With a bandgap energy (1.5 eV) that nearly matches the solar spectrum, CdTe-based solar cell efficiencies as high as 15.8% have been reported for small-area cells (1.08 cm²).[1] Industry has extended this bench-scale technology into the development of CdTe solar cell modules with efficiencies nearing 10% and output power densities approaching 100 W/m² of solar cell material.[2] In the calendar year 1995, 1.3 MW of CdTe solar-cell modules were shipped to customers thereby comprising 1.6% of the world-wide PV market.[3] Nearly all thin-film CdTe solar cells are composed of a multilayer structure with a p-type CdTe/n-type CdS heterojunction as the active part of the device. This cell structure was first fabricated in 1969 by Adirovich et al. using an evaporation technique and afforded a 1% efficient CdTe/CdS solar cell.[4] Other components of this now common CdTe device heterostructure include a
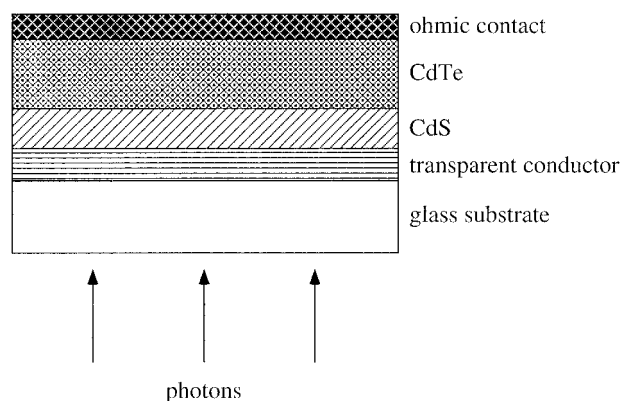
Figure 1. Schematic diagram of a typical CdTe thin-film solar cell.

transparent glass substrate, a transparent conducting layer, and a back electrode material. A schematic diagram of the typical CdTe thin-film solar cell is shown in Figure 1.

Several different deposition strategies have been employed by industrial companies for the growth of the CdTe absorber layer. These include techniques such as close-spaced sublimation, atomic layer epitaxy, elec-

(1) Ferekides, C.; Britt, J.; Ma, Y.; Killian, L. *Proc. 23rd IEEE Photovoltaic Spec. Conf.* **1993,** 389−393.
(2) Zweibel, K. *Prog. Photovoltaics: Res. Appl.* **1995,** *3,* 279−293.
(3) Maycock, P. D. *PV News* **1996,** *15* (2), 4.

(4) Adirovich, E. I.; Yuabov, Y. M.; Yagudaev, G. R. *Sov. Phys. Semiconduct.* **1969,** *3,* 61−64.

Table 1. Performance of CdTe Thin Film Solar Cell Modules

company	deposition method	area (cm²)	efficiency (%)	power (W)	ref
Solar Cells Inc.[a]	close-spaced sublimation	7200	8.4	60.3	2
BP Solar[b]	electrodeposition	4540	8.4	38.2	2
Golden Photon Inc.[c]	spray deposition	3341	8.5	28.4	6
Matsushita Battery[d]	screen printing	1200	8.7	10.0	2

[a] Solar Cells Inc., 1702 N. Westwood Ave., Toledo, OH 43607. [b] BP Solar, 12 Brooklands Close, Sunbury-on-Thames, Middlesex TW16 7DX, UK. [c] Golden Photon Inc., 4545 McIntyre St., Golden, CO 80401. [d] Matsushita Battery Industrial Co., Ltd., Matsusita-cho, Osaka 570, Japan, 06-991-1141.

trodeposition, screen printing, and spray deposition.[5] Spray deposition has several processing advantages such as the simplicity of the apparatus (no vacuum systems), manufacturability, and low processing costs. Toward this end, industrial researchers at Golden Photon, Inc., have successfully produced 28.4 W CdTe thin-film modules (active area = 2780 cm²; 10.2% active area efficiency; 7.6% total area efficiency) using a spray deposition approach for the growth of the CdTe layer.[6] Table 1 shows performance data for CdTe thin-film modules larger than 1000 cm² fabricated by industrial entities world-wide.

There have been relatively few reports of spray deposition of CdTe materials.[7–14] While knowledge of the CdTe spray deposition precursor chemistry in much of this work is unpublished,[7,10–12] a few reports document the composition of the spray solution. Aqueous precursor solutions of $(NH_4)_2TeO_4$, $CdCl_2$, and HCl[14] or TeO_2, $CdCl_2$, NH_4OH, N_2H_4, and HCl[9] have been sprayed at temperatures from 350 to 500 °C in the deposition of CdTe thin films. Weng and Cocivera have reported a three-step spray deposition route to CdTe as follows: first, a CdO film is spray deposited from an aqueous $Cd(NO_3)_2$ solution; second, the CdO is reacted with sulfur vapor to form CdS; third, the CdTe film is formed by reaction of tellurium vapor with the CdS film.[13] No CdTe devices were fabricated in any of these three reports.[9,13,14]

In 1981, Serreze et al. fabricated a very small area (2.4 mm²) CdTe/CdS solar cell with an efficiency of 4.0%.[7] This was the first documentation of a CdTe/CdS solar cell where the CdTe layer was deposited by spray deposition. The authors reported the use of Cu or As as p-type dopants for the CdTe layer and a carbon paste/Au metal back contact.[7] Subsequently, researchers at Photon Energy Inc. (now Golden Photon Inc.) reported a 12.7% efficiency for small-area (30.2 mm²) spray-deposited CdTe solar cells.[11,12] Dopants such as P and Cu were introduced into the CdTe layer and a graphite/Sn metal back contact was used. The fabrication of larger CdTe solar cells using the same process produced

modules with active area (754 cm²) efficiencies up to 8.1% and a 6.1 W power output.[11,12]

The past two decades have paid witness to the advent of the science of semiconductor nanoparticle materials.[15–18] As the diameter of a crystallite is reduced to the nanometer scale, physicochemical properties change from those of the bulk material to something approaching those of distinct molecules. The reduced dimensionality of these nanoparticle systems produce materials with novel properties such as an optical quantum size effect,[19,20] size-dependent chemical reactivity,[21,22] enhanced photoredox chemistry,[23] and optical nonlinearity.[24,25] Some of these properties have been utilized in the design of novel photoelectrochemical devices based upon surface-derivatized nanoparticle films.[26–29] In the design of these photoelectrodes, colloids are deposited onto substrates giving high surface area, porous films composed of nanoparticle crystallites. This has led to the design of a composite device which exhibits a solar-to-electric energy conversion efficiency of 10%.[30]

Another property associated with nanoparticles is a reduction in melting point versus the bulk material.[31] Alivisatos et al. have provided TEM selected area diffraction evidence that semiconductor nanoparticles exhibit reduced melting temperature with decreasing particle size.[31] In the reported study, CdS nanoparticles with a 40 Å diameter were observed to melt at a temperature of about 627 °C. This reduction in melting temperature is quite significant compared to the bulk melting temperature for CdS of 1405 °C. Reports of the formation of semiconducting bulk films derived from

(5) Suntola, T. *MRS Bull.* **1993**, *10*, 45–47 and references therein.
(6) Albright, S. P., personal communication.
(7) Serreze, H. B.; Lis, S.; Squillante, M. R.; Turcotte, R.; Talbot, M.; Entine, G. *Proc. 15th IEEE Photovoltaic Spec. Conf.* **1981**, 1068–1072.
(8) Feldman, B. J.; Boone, J. L.; Doren, T. v. *Appl. Phys. Lett.* **1981**, *38*, 703–705.
(9) Boone, J. L.; Doren, T. P. v.; Berry, A. K. *Thin Solid Films* **1982**, *87*, 259–264.
(10) Jordan, J. F.; Albright, S. P. *Solar Cells* **1988**, *23*, 107–113.
(11) Albright, S. P.; Jordan, J. F.; Ackermann, B.; Chamberlin, R. R. *Solar Cells* **1989**, *27*, 77–90.
(12) (a) Albright, S. P.; Ackermann, B.; Jordan, J. F. *IEEE Trans. Electron Dev.* **1990**, *37*, 434–437. (b) Albright, S. P.; Ackerman, B.; Chamberlin, R. R.; Jordan, J. F. NREL Subcontract Report No. ZN-9-19019, 1992; National Renewable Energy Laboratory, Golden, CO.
(13) Weng, S.; Cocivera, M. *Chem. Mater.* **1993**, *5*, 1577–1580.
(14) Khan, S. U. M.; Zhang, S. *J. Electrochem. Soc.* **1995**, *142*, 2539–2544.

(15) Steigerwald, M. L.; Brus, L. E. *Annu. Rev. Mater. Sci.* **1989**, *19*, 471–495 and references therein.
(16) Weller, H. *Adv. Mater.* **1993**, *5*, 88–95 and references therein.
(17) Weller, H. *Angew. Chem., Int. Ed. Engl.* **1993**, *32*, 41–53 and references therein.
(18) Service, R. F. *Science* **1996**, *271*, 920–922.
(19) Brus, L. E. *J. Chem. Phys.* **1983**, *79*, 5566–5571.
(20) Nozik, A. J.; Williams, F.; Nenadovic', M. T.; Rahj, T.; Mic'ic', O. *J. Phys. Chem.* **1985**, *89*, 397–399.
(21) Richtsmeier, S. C.; Parks, E. K.; Liu, K.; Pobo, L. G.; Riley, S. J. *J. Chem. Phys.* **1985**, *82*, 3659–3665.
(22) Beck, D. D.; Siegel, R. W. *J. Mater. Res.* **1992**, *7*, 2840–2845.
(23) Nedeljkovic', J. M.; Nenadovic', M. T.; Mic'ic', O. I.; Nozik, A. J. *J. Phys. Chem.* **1986**, *90*, 12–13.
(24) Wang, Y.; Mahler, W. *Opt. Commun.* **1987**, *61*, 233–236.
(25) Banyai, L.; Hu, Y. Z.; Lindberg, M.; Koch, S. W. *Phys. Rev. B* **1988**, *38*, 8142–8153.
(26) Hodes, G.; Howell, I. D. J.; Peter, L. M. *J. Electrochem. Soc.* **1992**, *139*, 3136–3140.
(27) Hodes, G. *Isr. J. Chem.* **1993**, *33*, 95–106 and references therein.
(28) Vinodgopal, K.; Hotchandani, S.; Kamat, P. V. *J. Phys. Chem.* **1993**, *97*, 9040–9044 and references therein.
(29) Vinodgopal, K.; Hua, X.; Dahlgren, R. L.; Lappin, A. G.; Patterson, L. K.; Kamat, P. V. *J. Phys. Chem.* **1995**, *99*, 10883–10889 and references therein.
(30) Nazeeruddin, M. K.; Kay, A.; Rodicio, I.; Humphry-Baker, R.; Müller, E.; Liska, P.; Vlachopoulos, N.; Grätzel, M. *J. Am. Chem. Soc.* **1993**, *115*, 6382–6390.
(31) Goldstein, A. N.; Echer, C. M.; Alivisatos, A. P. *Science* **1992**, *256*, 1425–1427 and references therein.

nanoparticle precursors utilizing the reduced melting point phenomenon have been published and patented.[32,33]

The use of nanoparticle precursors for thin-film spray deposition might offer several advantages over conventional spray deposition. As a consequence of higher surface diffusivities[34] and the reduction in melting temperature, nanoparticle precursor routes potentially offer lower processing temperatures. Decreased growth temperatures might allow the use of low-cost substrates such as soda-lime glass while alleviating substrate outdiffusion and relieving thermal stress. In addition, the improved packing during deposition inherent with the small particle diameter can produce smoother, denser films. This approach has the potential to yield films similar in quality to those obtained by vacuum techniques but without the expense and complexity.

We have recently reported the spray deposition of CdTe films using a nanoparticle CdTe colloid precursor.[35-37] The reduced melting temperature associated with nanoparticles was utilized in the reported studies with phase-pure CdTe film development observed at temperatures as low as 240 °C. These routes to CdTe films suffered from substantial C contamination, likely due to the nonvolatile trioctylphosphine (TOP) and/or trioctylphosphine oxide (TOPO) nanoparticle surface-capping agents. In this paper, we report the synthesis and characterization of methanol-capped CdTe nanoparticles and the use of these nanoparticles as precursors to CdTe thin-film growth by spray deposition. These CdTe thin films show a reduction in film contamination versus the TOP/TOPO-capped precursors. We expect the technology presented in this article should be transferable directly to the CdTe solar cell device community.

Experimental Section

Standard Schlenk techniques and a helium-filled Vacuum Atmospheres glovebox were used in the isolation and handling of CdTe nanoparticles. Spray deposition was performed in a nitrogen-purged Plas-Lab 818-GB glovebox fitted with an evacuable antechamber. Methanol solvent was dried over magnesium methoxide and was distilled immediately prior to use. Toluene solvent was dried over Na benzophenone ketyl radical while butanol and acetonitrile solvents were dried over calcium hydride. All solvents were distilled under nitrogen gas prior to use and were degassed with nitrogen gas for at least 15 min prior to experimentation. Glassware used in synthesis of CdTe nanoparticles was heated at 140 °C in a convection oven and was removed immediately into a Vacuum Atmospheres glovebox antechamber. Na_2Te was prepared by reaction of sodium metal with tellurium metal in liquid ammonia,[38] while CdI_2 (99.999%, Aldrich) was dried at 110 °C under dynamic vacuum overnight.

Optical properties of methanol-capped CdTe nanoparticles were determined in dilute butanol or toluene solutions with a Cary 5E UV–vis spectrophotometer in air-free quartz cuvettes. Photoluminescence (PL) measurements of methanol colloids were made with the 488 nm line from a continuous-wave Ar^+-ion laser using a spot size of ~200 μm. The PL was collected using a lens with NA = 0.25 and directed to a 0.27 m single spectrometer. A liquid nitrogen cooled CCD detected the dispersed PL signal. Crystalline phase formation of the nanocrystalline powder and the CdTe thin films was determined by XRD using a Rigaku DMAX-A instrument with a rotating Cu Kα anode. Average particle sizes were calculated according to the Scherrer equation[39] with an instrumental broadening factor determined using a LaB_6 standard (SRM 660). TEM was performed on CdTe nanoparticles using a Phillips CM30 operating at 300 kV. TEM samples were prepared by sonicating air-free toluene or acetonitrile slurries for 15 min prior to transfer into a nebulizer and spraying onto 100 Å amorphous carbon coated 200 mesh Mo grids in a standard fume hood. Thermogravimetric analysis (TGA) of the nanoparticles was carried out using a TA Instruments TGA 51 thermogravimetric analyzer with a Pt sample pan and N_2 carrier gas. CdTe thin-film morphologies were determined by AFM using an Autoprobe LS (Park Scientific Instruments) with silicon cantilevers. XPS data were collected using a Physical Electronics 5600 MultiTechnique.

CdTe nanoparticle colloids were prepared by the reaction of Na_2Te with CdI_2 in methanol by modification of a literature preparation.[40,41] Accordingly, 1.033 g of CdI_2 (2.82 mmol) was added to a 500 mL sidearm round-bottom flask fitted with a magnetic stir bar and 0.502 g Na_2Te (2.89 mmol) added to a 250 mL sidearm round-bottom flask fitted with a magnetic stir bar. Approximately 250 and 30 mL dried, degassed methanol was then added to the CdI_2 and Na_2Te flasks, respectively. Both flasks were subjected to vigorous stirring until the Na_2Te reagent was dissolved with the CdI_2 reagent dissolving only partially. Both flasks were cooled to −78 °C by employing dry ice/2-propanol baths with continued vigorous stirring. After a 25 min cooling period, the Na_2Te solution was added quickly to the CdI_2 mixture using a large bore cannula while maintaining the maximum stirring rate. The mixture became dark red immediately after addition and was allowed to warm with stirring. After the mixture warmed above 0 °C, stirring was ceased and the precipitate was allowed to settle. The colorless NaI in methanol supernatant was decanted via cannula and discarded. The remaining red slurry (~5−10 mL) was transferred to two 50 mL centrifuge tubes. The volumes in the centrifuge tubes were adjusted to 45−50 mL by the addition of fresh methanol. After sonication for 15 min, the tubes were centrifuged at 4000 rpm for 10 min. The clear supernatant was decanted via cannula and discarded. Addition of approximately 50 mL of methanol to the centrifuge tubes followed by sonication for 15 min afforded CdTe colloidal suspensions. Yields for this metathesis reaction are typically greater than 90%, with no stoichiometric adjustment made for the capping agent. An excess of the tellurium reagent, Na_2Te, ranging from 4 to 9 atom % was employed with overall reaction molarities from 14.5 to 15.9 mM with respect to CdI_2. CdTe nanoparticles prepared via this route shall be referred to as "methanol-capped". When stored under inert conditions, these CdTe nanoparticle colloids are stable for weeks.

An additional metathesis reaction was performed using a reaction temperature of 25 °C with all other conditions similar to the aforementioned experimental method. After addition of the Na_2Te solution to the CdI_2 mixture, a black precipitate was immediately observed. The CdTe material formed at 25 °C was characterized by TEM (see below). Although all thin-film precursor colloids employed in this study were methanol-capped, an alternative coordinating solvent, acetonitrile, has

(32) Chemseddine, A.; Fearheiley, M. L. *Thin Solid Films* **1994**, *247*, 3−7.

(33) Alivisatos, A. P.; Goldstein, A. N. United States Patent 5,262,-357, 1993.

(34) Andres, R. P.; Averback, R. S.; Brown, W. L.; Brus, L. E.; Goddard, W. A.; Kaldor, A.; Louie, S. G.; Moscovits, M.; Peercy, P. S.; Riley, S. J.; Siegel, R. W.; Spaepen, F.; Wang, Y. *J. Mater. Res.* **1989**, *4*, 704−736.

(35) Pehnt, M.; Schulz, D. L.; Curtis, C. J.; Jones, K. M.; Ginley, D. S. *Appl. Phys. Lett.* **1995**, *67*, 2176−2178.

(36) Pehnt, M.; Schulz, D. L.; Curtis, C. J.; Moutinho, H. R.; Schwartzlander, A.; Ginley, D. S. *Mater. Res. Soc. Symp. Proc.*, in press.

(37) Schulz, D. L.; Curtis, C. J.; Pehnt, M.; Ginley, D. S. *Proc. ISMANAM-95*, submitted for publication.

(38) Schultz, L. D.; Koehler, W. H. *Inorg. Chem.* **1987**, *26*, 1989−1993.

(39) Cullity, B. D. *Elements of X-ray Diffraction*; Addison-Wesley: Reading, 1978.

(40) Jarvis, R. F.; Müllenborn, M.; Yacobi, B. G.; Haegel, N. M.; Kaner, R. B. *Mat. Res. Soc. Symp. Proc.* **1992**, *272*, 229−234.

(41) Müllenborn, M.; Jarvis, R. F.; Yacobi, B. G.; Kaner, R. B.; Coleman, C. C.; Haegel, N. M. *Appl. Phys. A* **1993**, *56*, 3217−3221.

Table 2. Processing Conditions and Characterization of Spray Deposited CdTe Thin Films

film ID	substrate	deposition method	T_{dep} (°C)	annealing ambient	T_{anneal} (°C)	t_{anneal} (min)	CdCl$_2$[g] (%)	XRD phases[h]	XRD fwhm[d] (deg)	XRD grain size (Å)[e]	AFM area (mm^2)	AFM roughness (Å)[f]	AFM grain size (nm)[i]
280	7059 glass	one-step	280					A (br)	1.70	50			
350	7059 glass	one-step	350					A ≫ B	0.70	120			
400	7059 glass	one-step	400					A > B	0.45	200	6.56	437	100−300
440	7059 glass	one-step	440					A > B	0.35	280			
250-HN	7059 glass	two-step	125	forming[b]	250	100[c]		A(br) ≫ C	0.70	120			
300-HN	7059 glass	two-step	125	forming[b]	300	100[c]		A ≫ C	0.30	430			
400-HN	7059 glass	two-step	125	forming[b]	400	100[c]		A	0.20	>1000	5.38	514	350−700
500-HN	7059 glass	two-step	125	forming[b]	500	100[c]		A	0.20	>1000			
500-HNR	7059 glass	two-step	25	forming[b]	500	100[c]		A	0.70	120			
300-AR	7059 glass	two-step	125	argon	300	100[c]		A ≫ C	0.50	180			
400-AR	7059 glass	two-step	125	argon	400	100[c]		A	0.20	>1000			
400-HNCL	7059 glass	two-step	125	forming[b]	400	30[c]	10	A	0.20	>1000			
400-ARCL	7059 glass	two-step	125	argon	400	30[c]	10	A	0.20	>1000			
C1	composite[a]	one-step	400					A ≫ D	0.20	>1000			
C2	composite[a]	two-step	125	argon	400	100[c]		A ≫ D	0.20	>1000	6.37	590	100−300
C3	composite[a]	two-step	125	argon	400	100[c]	10	A ≫ D	0.20	>1000	5.74	611	300−400
C4	composite[a]	two-step	125	argon	400	100[c]	20	A ≫ D	0.20	>1000	5.90	725	800−1400

[a] CdS/SnO$_2$/7059 glass. [b] 10% H$_2$ in N$_2$. [c] With furnace cool. [d] Full width at half-maximum of the (111) reflection. [e] Diameter calculated using the Scherrer equation. [f] Root mean square. [g] Percentage versus saturated (i.e., 0.082 M) CdCl$_2$ in methanol solution. [h] Phase formation is denoted with the following abbreviations: A = cubic CdTe, B = CdTe$_2$O$_5$, C = Te metal, D = unknown, (br) = broad. [i] Grain size refers to diameter.

also been successfully employed to form stable CdTe nanoparticle colloids.[42]

Prior to spray deposition, the nanoparticle solution was loaded into a Paasche VL-Set airbrush and sonicated for 20 min to reduce agglomeration of the nanoparticles. The solution was then transferred to the Plas-Labs glovebox and sprayed onto heated substrates using nitrogen (10 L/min) as a carrier gas. Two types of substrates were used in this study. The first set of substrates were Corning 7059 glass which were prepared for deposition as follows: first, the substrates were sonicated for 10 min in a 5% Liquinox in distilled water solution; second, the substrates were rinsed five times with distilled water; third, the substrates were sonicated five times in distilled water; finally, the substrates were dried under a stream of nitrogen. The second set of substrates were comprised of a composite structure of a CdS layer on top of commercially obtained SnO$_2$-coated 7059 Corning glass (Solarex). The CdS films were prepared by chemical bath deposition according to a modification of the literature synthesis.[43] Specifically, the SnO$_2$ (hyp.) coated substrates were placed in a stirred and covered jacketed beaker at 89 °C with 550 mL of water, 8 mL of 0.033 M cadmium acetate, 5.3 mL of 1 M ammonium acetate, 15 mL of stock (30%) ammonium hydroxide, and 8 mL of 0.067 M thiourea (added in four 2 mL aliquots with 10 min interval). The resultant CdS films were 1000 Å thick and highly adherent and had an index of refraction of 2.3. CdTe was then spray deposited onto the CdS film to form the composite structure CdTe/CdS/SnO$_2$/7059.

Two deposition approaches were employed in this study, one step and two step. In the one-step method, the CdTe nanoparticle colloid was sprayed onto substrates heated to relatively high temperatures (T_{dep} = 280−440 °C) with no further thermal treatment. For these CdTe samples, film growth occurs as the preformed CdTe nanoparticles, upon interaction with the hot substrate, coalesce to form a CdTe thin film. A schematic diagram of the sprayer system employed for both the one- and two-step methods is shown in Figure 2. CdTe films obtained by a two-step approach were produced by first spraying the CdTe nanoparticle colloid onto substrates at relatively low temperatures (T_{dep} = 25−125 °C) and then subjecting these "green" precursor films to a subsequent thermal treatment. Samples were annealed (T_{anneal} = 250−500 °C) under flowing argon or flowing forming gas (10% H$_2$ makeup N$_2$) ambients with a fixed flow rate of 160 mL/min.

(42) Schulz, D. L.; Curtis, C. J.; Pehnt, M.; Ginley, D. S. Patent application on file, 1995.
(43) Froment, M.; Bernard, M. C.; Cortes, R.; Mokili, B.; Lincot, D. *J. Electrochem. Soc.* **1995**, *142*, 2642−2649 and references therein.
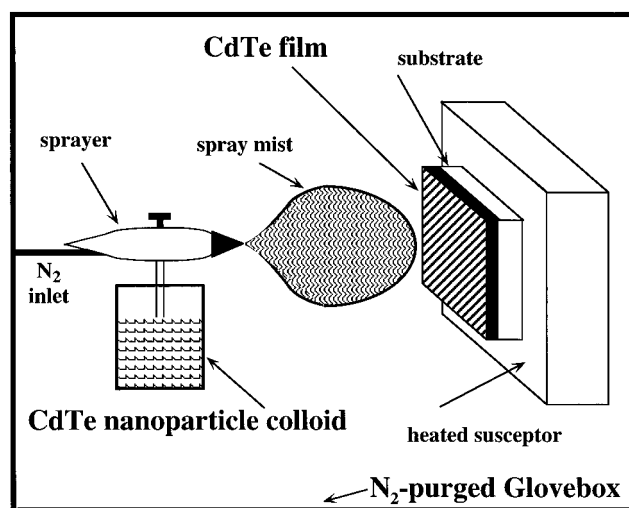
Figure 2. Schematic diagram of the spray deposition system employed in this study.

Films were introduced into a preheated Lindberg tube furnace and annealed for 100 min prior to slow cooling of the samples realized by turning off the furnace power. The deposition processing conditions are summarized in Table 2. For both the one- and two-step methods, the distance from the sprayer nozzle to the substrate was adjusted such that initial impingement of the colloid spray onto the heated substrate led to wetting of the substrate followed by rapid evaporation of the methanol solvent. Upon spraying too close to the substrate, the ink tended to run giving poor film morphologies. Spraying too far from the substrate provided no film growth due to premature solvent evaporation and the subsequent low sticking coefficient of dry nanoparticles.

The effects of a CdCl$_2$ treatment on CdTe film properties were probed by treating two-step processed films prior to postannealing. Accordingly, CdTe precursor films sprayed at 125 °C were dipped in 10 or 20% saturated methanol solutions of CdCl$_2$ at 50 °C for 5 min prior to the annealing process. These CdCl$_2$-treated CdTe precursor films were annealed at 400 °C for 30 min in either flowing argon or forming gas followed by furnace cooling to room temperature (Note: this CdCl$_2$ annealing scheme differs from the remainder of the films in this study which were annealed for 100 min). The effects of CdCl$_2$ treatment on the composite structure CdTe/CdS/SnO$_2$/7059 were probed by performing the aforementioned CdCl$_2$ treatment on the composite structure films and then annealing
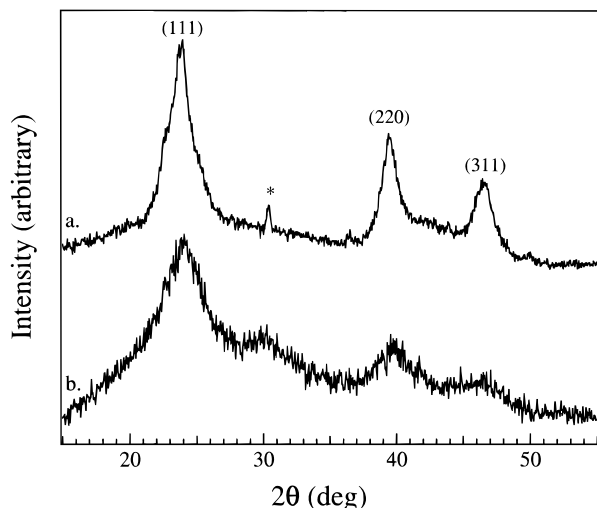
Figure 3. XRD $\theta/2\theta$ data for CdTe nanoparticles prepared by (a) methathesis reaction of CdI_2 with Na_2Te in methanol; and, (b) reaction of $Cd(CH_3)_2$ with TOPTe in TOP/TOPO (* denotes an oxide phase).

Figure 4. UV-vis spectra of CdTe nanoparticles in dilute butanol solution prepared by (a) methathesis reaction of CdI_2 with Na_2Te in methanol and (b) reaction of $Cd(CH_3)_2$ with TOPTe in TOP/TOPO.

in argon at 400 °C for 100 min with subsequent furnace cooling.

Results and Discussion

A. Nanoparticles. Figure 3 shows the XRD pattern for two different CdTe nanoparticle powders. The XRD spectrum for CdTe nanoparticles prepared by the low-temperature metathesis reaction of CdI_2 with Na_2Te is shown in Figure 3a. Three peaks are observed which correspond to the (111), (220), and (311) reflections of cubic zincblende CdTe (PDF No. 15-770). These peaks are broadened due to the nanosize particles with an approximate particle size of 44 Å calculated by applying the Scherrer equation to the (111) reflection (fwhm = 2.45°). Figure 3b shows the XRD spectrum for TOP/TOPO-capped CdTe nanoparticles prepared as previously reported.[35-37] Similar Scherrer equation analysis of the (111) reflection of the TOP/TOPO-capped CdTe (Figure 3b) gives a mean particle diameter of 28 Å. It is important to note that particle size analysis using the Scherrer equation tends to err toward distributions that are less than the true size as XRD emphasizes small crystallites while defective surface layers are not observed.

Apparent in the XRD pattern of the methanol-capped CdTe nanoparticles (Figure 3a) is a peak at $2\theta \sim 30°$ which corresponds to the strong reflections for each of the following phases; TeO_2 (paratellurite; PDF No. 11-693), α-$CdTeO_3$ (PDF No. 36-889), and $CdTe_2O_5$ (PDF No. 36-345). This oxide phase is likely a surface contaminant which forms upon exposure of the methanol-capped CdTe to air.[44] It is interesting to note that given identical handling of the two types of CdTe nanoparticles for the XRD characterization, the methanol-capped materials show evidence of surface reaction. This observation illustrates the relative stability of TOP/TOPO-capped versus methanol-capped CdTe nanoparticles.

Figure 4a shows the UV–vis spectrum of CdTe nanoparticles which were synthesized at −78 °C ac-

cording to the metathesis reaction and then examined in dilute butanol solution. The onset of the absorbance spectrum is shifted to shorter wavelengths (i.e., blue-shifted) versus the absorbance of bulk CdTe according to the quantum size effect. Also observable in many UV−vis spectra of nanoparticles is a shoulder which is caused by the first excitonic transition. As the energy levels of the excitonic transitions are a function of particle size, the position of these shoulders can be used to evaluate the particle size. The shoulder of this solution occurs at 570 nm (Figure 4a), as defined by the zero-point of the second derivative of the absorbance with respect to wavelength. Employing a tight-binding calculation,[45] this corresponds to an average particle size of 29 Å; a number which is smaller than the diameter obtained from the XRD data. Figure 4b shows the UV−vis spectrum of TOP/TOPO-capped CdTe nanoparticles in dilute butanol solution.[35] A blue shift is observed with an excitonic shoulder located at 548 nm corresponding to a particle size of 28 Å according to tight-binding calculations. Compared to the TOP/TOPO-capped nanoparticles, the shoulders are less pronounced in the methanol-capped CdTe nanoparticles. This difference in the UV−vis spectra is indicative of a broader size distribution in the latter versus the former. Photoluminescence data for a dilute methanol suspension of CdTe nanoparticles prepared at a reaction temperature of −78 °C showed a very weak emission at 850−865 nm. This low PL yield is likely a consequence of surface defects associated with this metathesis where the CdTe nanoparticles precipitate rapidly from solution. Also, methanol is expected to be a weakly bound capping ligand that does not passivate the surface sufficiently to observe strong band-edge PL.

Figure 5a shows a TEM image of methanol-capped CdTe nanoparticles prepared at a reaction temperature of −78 °C. CdTe nanoparticle diameters ranged from 25 to 75 Å as determined by measuring distinct particles at different positions on the TEM grid. It is also clear from the TEM analysis that the methanol-capped CdTe nanoparticles agglomerate. Characterization of the size

(44) Choi, S. S.; Lucovsky, G. *J. Vac. Sci. Technol. B* **1988**, *6*, 1198−1203.

(45) Lippens, P. E.; Lannoo, M. *Semiconduct. Sci. Technol.* **1991**, *6*, A157-A160.
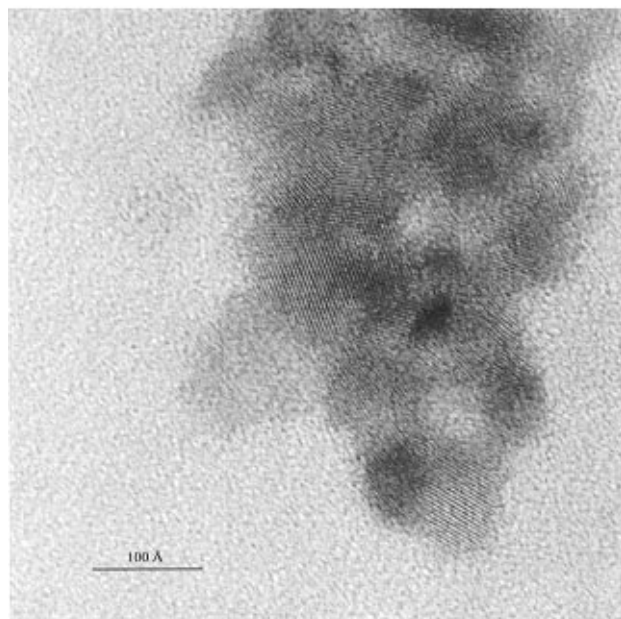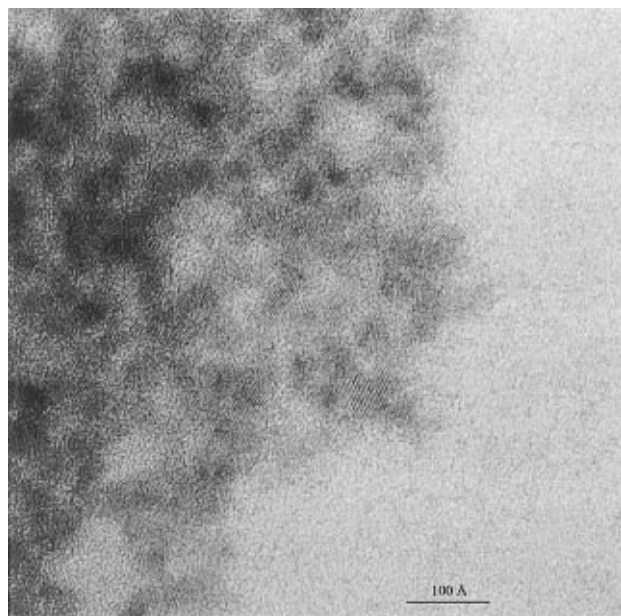
Figure 5. TEM lattice images of methanol-capped CdTe nanoparticles prepared by methathesis reaction of CdI₂ with Na₂Te in methanol at (a) −78 °C at 260K × magnification and (b) 25 °C at 340K × magnification.

distribution of the CdTe nanoparticles is severely complicated by this agglomeration. Figure 5b shows a TEM image of methanol-capped CdTe nanoparticles prepared in a fashion identical with those shown in Figure 5a except that the temperature for this reaction was 25 °C. CdTe particles with 9–23 lattice planes corresponding to diameters of 33–85 Å are observed (Figure 5b). It is also important to note that outside the range of this photo, a much larger size distribution is observed. The presence of larger particles is consistent with the associated black color of this colloid and expected for the elevated synthesis temperature. A wide size range for CdTe nanoparticles has been reported by Müllenborn et al., who employed a similar reaction strategy.[41]

Particle size distributions of 31–47[35] and 25–75 Å (see above) were determined by TEM for TOP/TOPO- and methanol-capped CdTe nanoparticles, respectively.
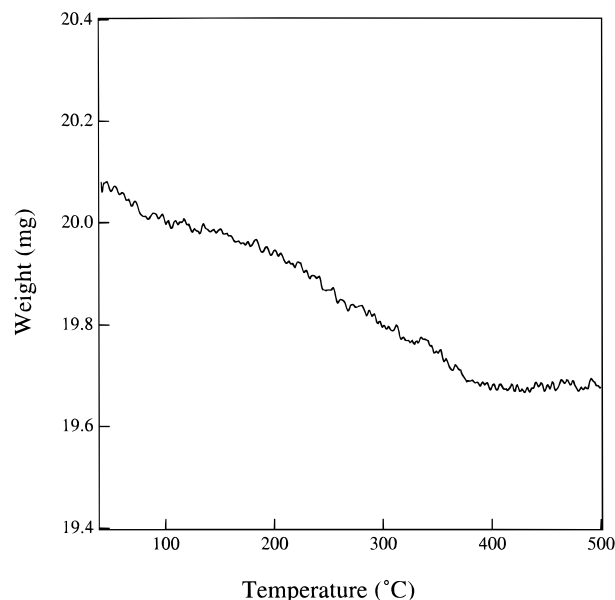
Figure 6. TGA data for CdTe nanoparticles prepared by methathesis reaction at −78 °C.

This observation might be explained owing to marked differences in the syntheses. For methanol-capped nanoparticles, CdI₂ is reacted with Na₂Te in methanol (eq 1) while TOP/TOPO-capped materials are formed

$$CdI_2 + Na_2Te \xrightarrow{CH_3OH,\ T \sim -78\ °C}$$
$$\text{methanol-capped CdTe} + 2NaI \quad (1)$$

$$Cd(CH_3)_2 + Te(TOP) \xrightarrow{TOPO,\ T > 54\ °C}$$
$$\text{TOPO-capped CdTe} + \text{byproducts} \quad (2)$$
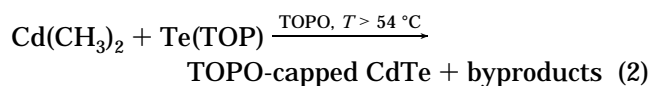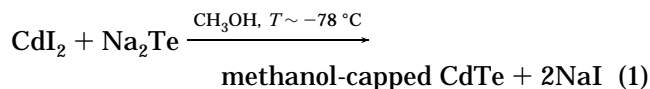
by the reaction of Cd(CH₃)₂ with Te(TOP) in molten TOP/TOPO (eq 2). While CdTe nanoparticle growth according to the TOP/TOPO-based synthesis has been described as "Ostwald ripening",[46] the growth details of the metathesis reaction reported herein are presently unknown but under investigation. Although a much broader size distribution is produced in the CdI₂-based synthesis, it possesses a marked economic advantage over the organometallic Cd(CH₃)₂-based synthesis. A synthetic advantage is also afforded for the CdI₂-based synthesis. Foremost is the simplicity associated with product isolation for CdTe nanoparticles formed via eq 1. Accordingly, the byproduct of the reaction, namely, 2 mol equiv of NaI, can be removed from the reaction mixture by simply decanting the methanol supernatant in which the NaI remains soluble. The methanol-capped CdTe nanoparticles are then reacted with a capping agent of choice to form a colloid.[42] By way of comparison, the isolation of TOP/TOPO-capped CdTe nanoparticles[46] according to eq 2 is quite tedious and difficult owing to the formation of oily byproducts.[47]

CdTe nanoparticles prepared by the methathesis reaction at −78 °C were further characterized by TGA. Figure 6 shows the thermogravimetric curve for a 20.08 mg sample heated at a rate of 20 °C/min under flowing N₂ (100 mL/min). A nearly linear rate of weight loss occurs from 25 to about 400 °C at which point a change

(46) Murray, C. B.; Norris, D. J.; Bawendi, M. G. *J. Am. Chem. Soc.* **1993**, *115*, 8706–8715.
(47) Schulz, D. L.; Curtis, C. J., unpublished results, 1995.
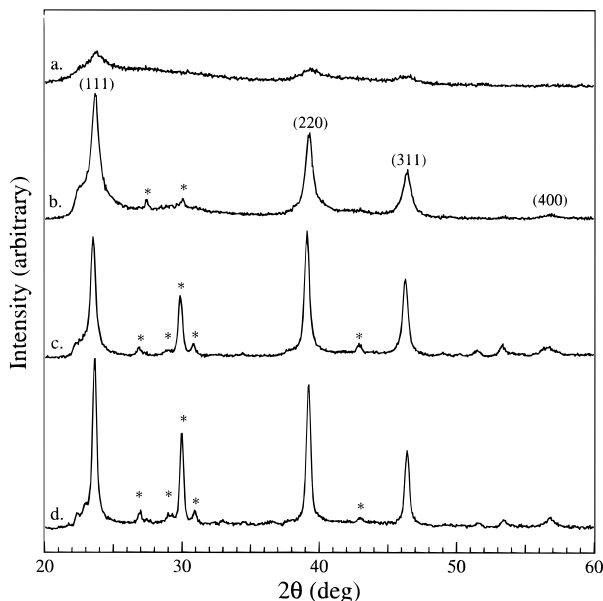
Figure 7. XRD $\theta/2\theta$ data of CdTe films deposited by the one-step approach using substrate temperatures of (a) 280, (b) 350, (c) 400, and (d) 440 °C (* denotes $CdTe_2O_5$).

in mass is no longer observed with a final mass of 19.72 mg, a 1.8% weight loss. This percentage weight loss is markedly different than that observed for TGA characterization of TOP/TOPO-capped CdTe nanoparticles where a 25% weight loss was observed by a temperature of 250 °C using an identical temperature ramp and carrier gas.[48] This observation is consistent with the higher molecular weight of a TOP/TOPO cap versus the methanol cap assuming weight loss is due to evolution of the capping agent and similar capping coverages. XRD analysis of the TGA residue of methanol-capped CdTe nanoparticles gave cubic CdTe formation with a (111) fwhm of 0.40° (vs 2.45° as-synthesized, see above) which implies sintering/coalescence of the nanoparticles.

B. CdTe Film Phase Development. XRD $\theta/2\theta$ patterns of CdTe films deposited by the one-step approach are shown in Figure 7. A significant increase of CdTe crystallinity with increasing deposition temperature is noted as follows: XRD full width at half-maximum (fwhm) values for the (111) peak decrease from 1.7° for film 280 (T_{dep} = 280 °C) to 0.35° for film 440 (T_{dep} = 440 °C). XRD results are summarized in Table 2. Also apparent in the XRD characterization of these one-step deposited films is the development of a contaminant oxide phase with several XRD reflections. While the strongest of these peaks at $2\theta \sim 30°$ may be attributed to paratellurite TeO_2 or α-$CdTeO_3$, the remainder of the reflections indicate the contamination phase is $CdTe_2O_5$ (PDF No. 36-345). An increase in the XRD intensity of the oxide phase occurs with increasing deposition temperature. The evolution of this phase may be a consequence of incomplete exclusion of air from the ink reservoir in the Paasche sprayer during sonication or from the nitrogen-purged spraying box. This oxide formation during one-step spraying of methanol-capped CdTe nanoparticle precursor colloids stands in contrast to the results using TOP/TOPO-capped CdTe nanoparticles where no tellurium/cadmium oxide phase formation was observed given a nearly identical one-
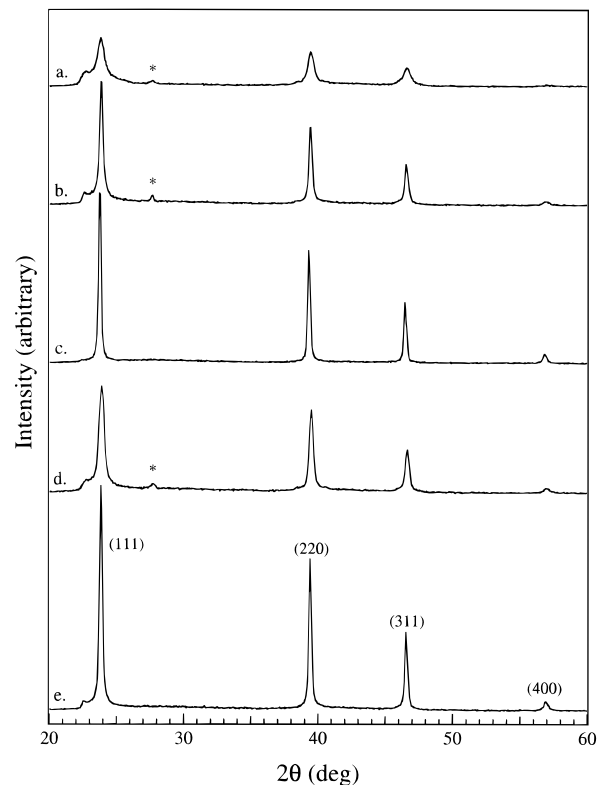
Figure 8. XRD $\theta/2\theta$ data for two-step deposited films sprayed at 125 °C and then annealed for 100 min in flowing forming gas at (a) 250, (b) 300, and (c) 400 °C or in argon at (d) 300 and (e) 400 °C (* denotes Te).

step spray deposition approach. This observation provides a measure of the relative stability of methanol-capped versus TOP/TOPO-capped CdTe nanoparticles as applied toward one-step spray deposition of CdTe films.

The XRD patterns for two-step deposited films sprayed at 125 °C and then annealed in forming gas at variable temperatures for 100 min are shown in Figure 8. The XRD pattern for film 400-HN (T_{anneal} = 400 °C; Figure 8c) gives a fwhm value of the (111) reflection equal to that of the XRD standard (i.e., natural line width) which indicates CdTe polycrystallite grain size diameters larger than 1000 Å comprising the film (see Table 2). By way of comparison, film 300-HN (T_{anneal} = 300 °C; Figure 8b) and film 250-HN (T_{anneal} = 250 °C; Figure 8a) exhibit fwhm of the (111) peak of 0.30° and 0.70°, respectively. These fwhm values correspond to Scherrer equation-derived grain sizes of 430 and 120 Å for films 300-HN and 250-HN, respectively. No contaminating cadmium/tellurium oxide phase is observed for these two-step derived films; however, a shoulder at $2\theta \sim 23°$ and a small peak at 27.6° are observed in films 250-HN and 300-HN. These peaks, attributed to metallic tellurium (PDF No. 36-1452), are not observed in the film annealed at 400 °C (Film 400-HN). The observation of tellurium in films 250-HN and 300-HN is consistent with the stoichiometric excess of Na_2Te employed in the synthesis of the nanoparticle CdTe precursor materials. Owing to the substantial vapor pressure of tellurium at 400 °C (i.e., 3.4 × 10⁻² Torr),[49] the disappearance of the tellurium reflections in the XRD of Film 400-HN (Figure 8c) is consistent with

(48) Pehnt, M. Diploma Thesis, Universität Tübingen, 1995.

(49) Brebrick, R. F. *J. Phys. Chem.* **1968**, *72*, 1032−1036.
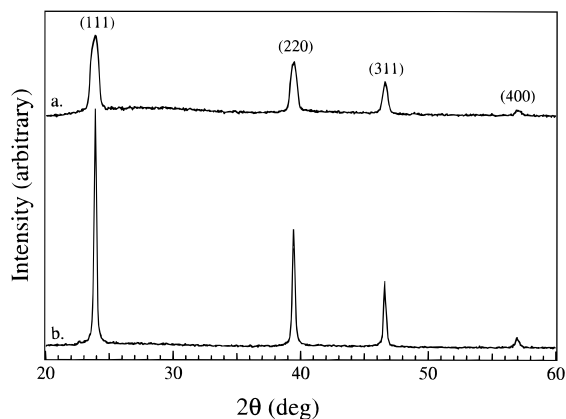
Figure 9. XRD $\theta/2\theta$ data for CdTe films annealed for 100 min at 500 °C in forming gas using precursor spray deposition temperatures of (a) 25 and (b) 125 °C.

vapor-phase evolution of tellurium from the film during the annealing step.

Two-step films annealed in argon exhibit phase development similar to the two-step films annealed in forming gas. Fwhm values for the (111) reflection of 0.50° and 0.20° are observed in the XRD $\theta/2\theta$ patterns for film 300-AR (T_{anneal} = 300 °C; Figure 8d) and film 400-AR (T_{anneal} = 400 °C; Figure 8e), respectively, and correspond to grain sizes of 180 and >1000 Å (see Table 2). The phenomenon of tellurium vaporization from the films annealed in argon is similar to the films annealed in forming gas. Accordingly, a peak at $2\theta \sim 27.6°$ corresponding to Te metal is observed in film 300-AR (Figure 8d) while this peak has disappeared in the XRD characterization of film 400-AR (Figure 8e), indicative of tellurium vaporization.

Spray deposition temperature has a pronounced effect on subsequent crystalline development in the two-step CdTe films. Figure 9 shows the XRD patterns for two films which were both annealed at 500 °C for 100 min in forming gas with one precursor film sprayed at a reduced temperature of 25 °C (T_{dep} = 25 °C; film 500-HNR; Figure 9a) and the other precursor film sprayed at 125 °C (T_{dep} = 125 °C; film 500-HN; Figure 9b). A marked difference in the XRD peak shapes for the two films is noted (Figure 9) with (111) fwhm values of 0.70° and 0.20° corresponding to grain sizes of 120 and >1000 Å for films 500-HNR and 500-HN, respectively (see Table 2). According to these data, it seems that some heating during initial deposition is required to form a precursor film which is amenable to subsequent large grain growth during sintering. It is possible that a spray deposition temperature of 25 °C is insufficient to promote complete evolution of the methanol solvent and/ or methanol-cap upon interaction with the substrate. As a consequence, inclusion of the solvent and/or capping agent within the precursor film might be expected as well as the formation of a noncontiguous film upon evolution of the trapped methanol species during post-deposition thermal treatment. While this explanation is quite speculative, the growth mechanism for transformation of capped-CdTe nanoparticles to CdTe films is currently being investigated.

The effects of a CdCl$_2$ treatment upon CdTe film properties were investigated due to the prevalence of this procedure among the CdTe device community. In general, annealing in the presence of CdCl$_2$ enhances grain growth in polycrystalline CdTe. In this study, CdCl$_2$ treatment has also been found to aid in the elimination of secondary phases and other ionic contaminants (see below). Two different CdCl$_2$ treatment annealing ambients were investigated, flowing argon and flowing forming gas. Compared to non-CdCl$_2$-treated films annealed under similar ambients, these treatments yielded similar phase formation (i.e., cubic CdTe and no residual metallic tellurium) for a given annealing temperature (e.g., 400-HNCL vs 400-HN and 400-ARCL vs 400-AR). It is interesting to note that this similar phase formation occurs in CdCl$_2$-treated films after only a 30 min anneal versus a 100 min anneal for nontreated films.

Phase development in the composite structure CdTe/CdS/SnO$_2$/7059 films subjected to various treatments was determined by XRD. Results from this characterization show that irrespective of the synthetic routes employed, major cubic CdTe phase formation is observed with fwhm values of the (111) reflection of 0.20° corresponding to grain sizes >1000 Å (Table 2). Also observed in all of these films are XRD reflections from impurity phases. While the identity of this minority phase, with maxima at about 51.6, 31.3, and 30.6° 2θ, remains undetermined, known PDF XRD patterns of likely phases (e.g., mixed phases containing Cd, Te, S, Sn, and O ions from the composite structure) do not match the observed patterns.

C. CdTe Film Surface Morphological Development. Surface morphologies of several films were measured using AFM. This characterization showed the CdTe films to be pinhole and crack free. Figure 10 shows AFM images of CdTe films processed at 400 °C according to both a one-step approach (Figure 10a; film 400) and a two-step approach using forming gas as the annealing ambient (Figure 10b; film 400-HN). The reported range of grain size, or grain agglomerate size, was determined by measuring the smallest and largest diameters in the AFM images. Grain sizes from about 100−300 nm are observed for the one-step film sprayed at 400 °C (Figure 10a), while 350−700 nm CdTe grains are observed for the film sprayed at 125 °C and annealed in forming gas at 400 °C for 100 min. AFM results are summarized in Table 2. While film 400-HN possesses larger grains, film 400 shows a smoother overall morphology with rms surface roughness values of 514 Å for the former versus 437 Å for the latter. The grain sizes determined by AFM for these two films are approximately 1 order of magnitude larger than those obtained using XRD techniques and held to be more representative of the true nature of morphological development.

AFM characterization was performed on several CdTe films on the CdS/SnO$_2$/7059 composite substrates. Figure 11 shows AFM images for two-step CdTe films sprayed at 125 °C which were annealed in argon for 100 min at 400 °C after various CdCl$_2$ treatments. Grain sizes of 100−300 nm are observed (Figure 11a; film C2) for the film subjected to no CdCl$_2$ treatment prior to argon annealing. Grain size seems to increase as a function of the concentration of the CdCl$_2$ treatment with other variables fixed. To this end, grain sizes ranging from 300 to 400 and 800−1400 nm are observed in the AFM images of CdTe films treated with 10% (Figure 11b; film C3) and 20% (Figure 11c; film C4)
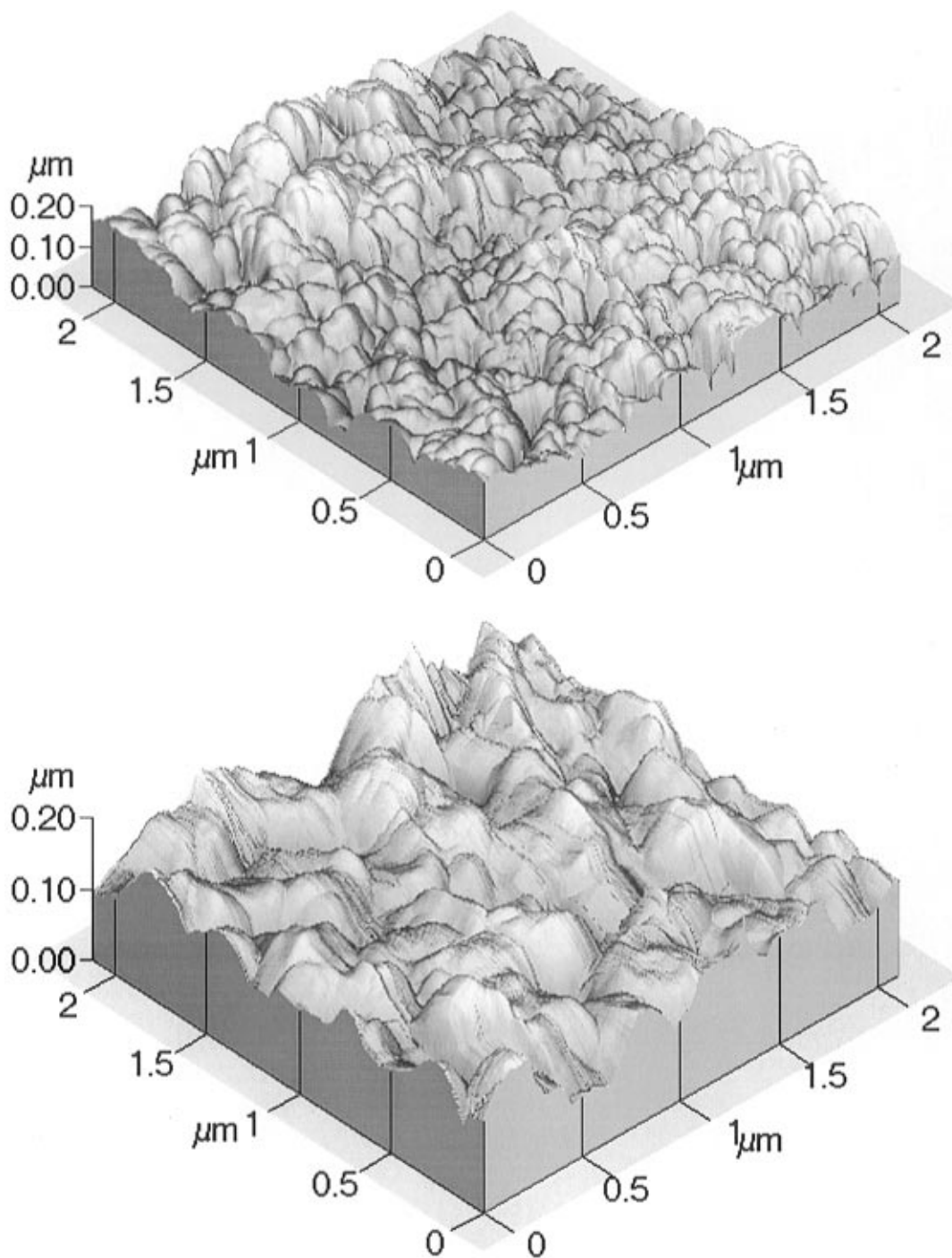
Figure 10. AFM images of CdTe films processed at 400 °C according to a (a) one-step approach; and (b) two-step approach using forming gas as the annealing ambient.

saturated CdCl$_2$ in methanol solutions, respectively. This AFM grain size data are consistent with those determined by XRD (Table 2). CdCl$_2$ treatments using >20% saturated solutions led to adhesion problems which were possibly due to loss of contact with the CdS layer during the grain growth/recrystallization of the CdTe layer. Optimization of this step is dependent upon film thickness as well as surface morphology (i.e., porosity) prior to CdCl$_2$ treatment.

D. CdTe Film Elemental Composition. The elemental compositions of the CdTe films were determined using XPS to probe film composition as a function of deposition method, annealing gas, and CdCl$_2$ treatment. Table 3 shows XPS data for CdTe films processed at 400 °C under a variety of conditions. The surface of each of these films was sputtered to a depth of 500 Å prior to data collection. There are several observations that are noteworthy regarding the chemical compositions of these films. First, Cd and Te are nearly stoichiometric for all films in Table 3. This likely relates to the nearly fixed Cd:Te ratio within the crystalline CdTe nanoparticle precursor. Second, while no C or Na is noted, an O contamination is observed for the film which was sprayed onto a substrate heated ($T_{dep} = 400$ °C) according to the one-step method (film 400). This observation is consistent with XRD data for this film (Figure 7c) and may be a consequence of the likely incomplete exclusion of air from the ink reservoir in the Paasche sprayer during sonication or from the nitrogen-purged spraying box. The use of a glovebox fitted with
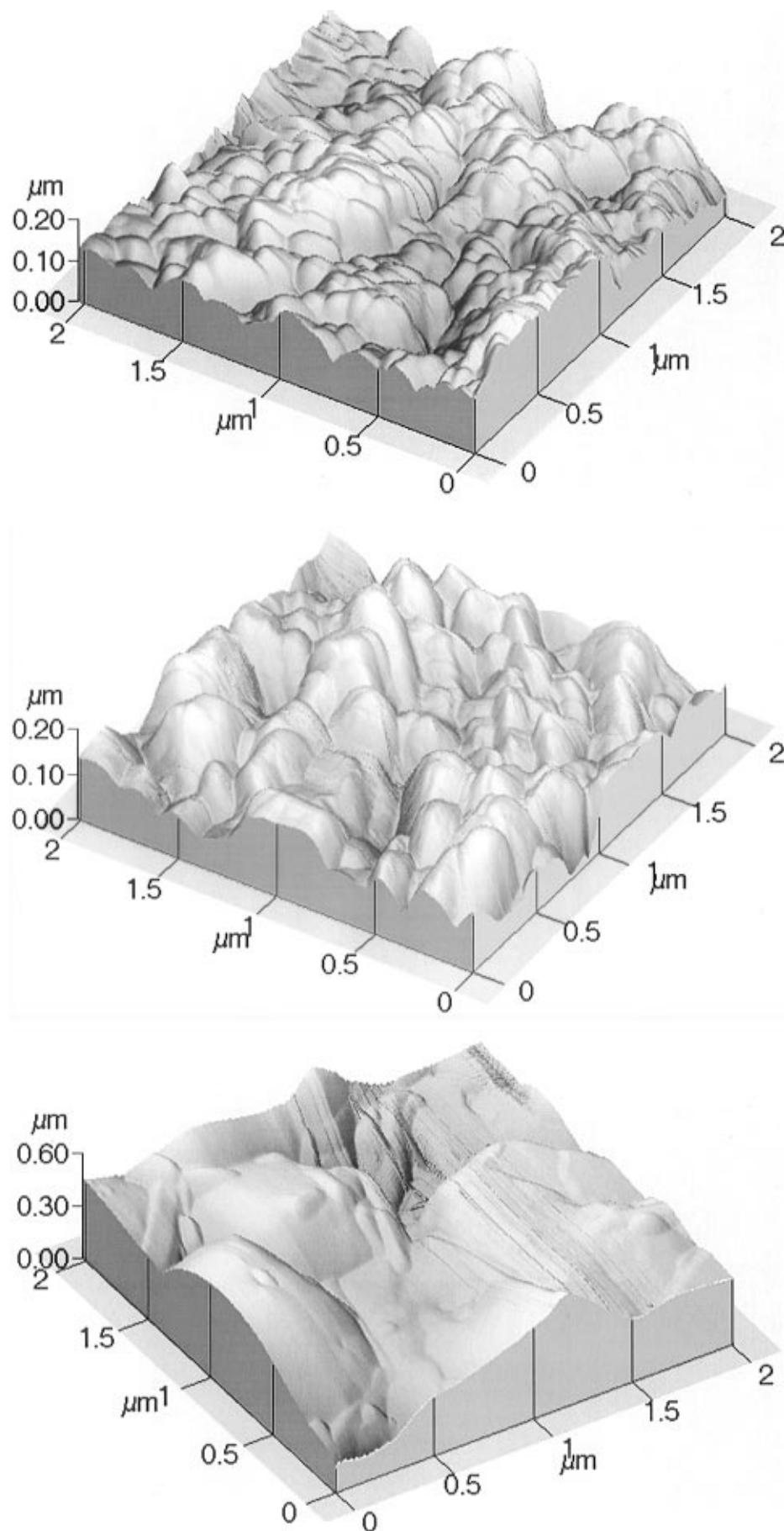
Figure 11. AFM images for two-step CdTe films sprayed at 125 °C which were annealed in Ar for 100 min at 400 °C after (a) no CdCl$_2$ treatment, (b) 10% saturated CdCl$_2$ in methanol treatment, and (c) 20% saturated CdCl$_2$ in methanol treatment.

CdTe Thin Films from Nanoparticle Precursors

Chem. Mater., Vol. 9, No. 4, 1997 **899**
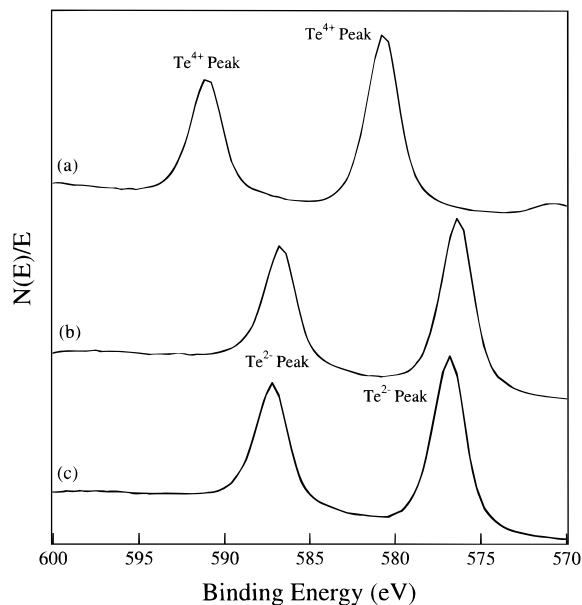
Figure 12. XPS data for film 400-HNCL (a) as-received, (b) after a 50 Å sputter treatment, and (c) after a 500 Å sputter treatment.

Table 3. XPS Data of CdTe Films Processed at 400 °C

film ID	atomic %					weight %				
	Cd	Te	C	O	Na	Cd	Te	C	O	Na
400	40	38	0	22	0	46	50	0	4	0
400-HN	25	23	21	24	7	43	45	4	6	2
400-HNCL	40	41	15	4	0	45	52	2	1	0
400-AR	20	21	20	29	11	38	46	4	8	4
400-ARCL	41	42	13	4	0	45	52	2	2	0

an oxygen-removal catalyst is anticipated to reduce the O contamination levels in these one-step films. Third, substantial C contamination was noted for all two-step films; an observation in marked contrast to the one-step film (film 400) that contained no C. It is plausible that spray deposition at a lower temperature (i.e., 125 °C) lends itself to a condition where the organic solvent and/ or capping agent are trapped within the film bulk region in a manner such that evolution of these molecules is inhibited during subsequent postdeposition processing treatments. Fourth, $CdCl_2$ treatment of CdTe films prepared by the two-step method reduces the relative impurity levels versus nontreated films. To this end, Na contamination is completely eliminated for films 400-HNCL and 400-ARCL with a moderate and extreme reduction of C and O, respectively, versus films 400-HN and 400-AR (Table 3).

XPS analysis of the films in Table 3 showed two different sets of doublets for tellurium. Doublets at 577/ 587 and 581/592 eV corresponding to oxidation states of Te^{2-} and Te^{4+} were observed with Te^{2-} likely existing as CdTe and Te^{4+} as an oxide phase (e.g., TeO_2, $CdTeO_3$, or $CdTe_2O_5$). Figure 12 shows XPS data for film 400-HNCL. The XPS spectrum of the sample as received (Figure 12a) shows only a Te^{4+} peak. As the sample is sputtered to depths of 50 Å (Figure 12b) and 500 Å (Figure 12c), only the Te^{2-} peak is observed. The data presented in Figure 12 indicate that the oxide contamination is a surface reaction product in film 400-HNCL which may occur upon exposure of the film to ambient conditions in preparation for the XPS analysis. This CdTe surface oxide phenomenon has been previously documented.[44]
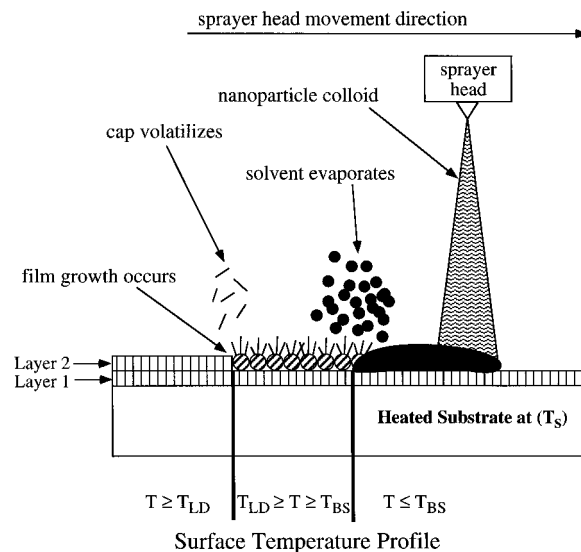
Figure 13. Schematic diagram of film growth via one-step spray deposition of a colloidal precursor which shows one possible layer-by-layer growth process. T corresponds to the temperature of the growth layer and T_S to the temperature of the substrate, while T_{LD} and T_{BS} are the temperature of ligand desorption and the boiling temperature of the solvent, respectively.

E. Growth Process Comment. Figure 13 is a schematic diagram of CdTe film growth via one-step spray deposition of a colloidal precursor showing one possible layer-by-layer growth process. Accordingly, pressurized CdTe colloidal ink is sprayed from a spray nozzle onto a heated substrate at elevated temperature (T_S) with the actual temperature of the growth layer given as T. The sprayer head traverses the substrate at a given rate at a distance from the substrate such that the surface becomes wetted initially. Heat from the substrate at T_S may be transferred to the growth layer until the temperature of the growth layer becomes equal to the boiling temperature of the solvent (i.e., $T \geq T_{BS}$). At this point, the solvent may evaporate leaving capped nanoparticles on the film surface. As more heat is transferred from the substrate to the growth layer, the growth layer temperature exceeds the temperature for ligand desorption (i.e., $T \geq T_{LD}$) and the cap may be volatilized with film growth occurring concomitantly.

According to this proposed layer-by-layer process, several variables exist with respect to overall film growth. First, the instantaneous cooling of the substrate is a function of the flow rates and heat capacities of the colloid and the carrier gas. These variables can be modified using different types of sprayer heads, solvents, or carrier gases. Second, the overall system pressure during film growth effects both the solvent evaporation and the cap volatilization processes. At lower pressures, the solvent evaporation and cap volatilization would occur at lower temperatures. Finally, the condition and heat capacity of underlying growth layers clearly affects the kinetics of the growth mechanism of subsequent layers.

The one-step process reported here is markedly different from reported two-step approaches. Chemseddine and Fearheiley reported the growth of CdS layers using a nanoparticle precursor route.[32] Accordingly, thiolate-capped CdS nanoparticles were first dissolved in dimethylformamide solvent. Thin-film growth was realized by simply depositing some drops of this solution

onto quartz substrates at ambient temperature and allowing the solvent to evaporate. Thermal treatment of the films led to phase pure CdS growth owing to capping ligand thermolysis. A noncontiguous, quantum wire-type microstructure was observed upon thermal treatment of the "green" precursor film. From a device processing perspective, this morphological development would be a limitation of this approach. Alivasatos and Goldstein have patented a route to low-temperature thin films formed from nanocrystal precursors according to a two-step approach.[33] According to this process, a contiguous layer of nanocrystals are first deposited onto a substrate and then fused together at a temperature below the bulk melting point of the semiconducting compound. It is reported, however, that thicker layers (>30 particles deep) begin to act as bulk materials and do not fuse at lower temperatures.[33] The one-step route we have established is not limited by the development of nonideal morphologies or by the loss of melting point reduction associated with the aforementioned two-step processes. As a consequence, we envision this one-step approach should be amenable to a wide variety of electronic materials; limited only by the ability to synthesize a nanoparticle precursor colloid of the material of interest. In the short term, we hope to extend this methodology to the industrial synthesis of CdTe-based solar cells.

Conclusions

Nanoparticle CdTe colloids have been synthesized by reacting CdI_2 with Na_2Te in methanol solvent. The reaction temperature affects the nanoparticle size distribution with lower temperatures leading to smaller nanoparticles as determined by XRD, UV–vis, and TEM. While methanol-capped nanoparticle CdTe materials exhibit less stability toward oxidation than other materials such as TOP/TOPO-capped CdTe, the evolution of the capping agent seems to occur much more readily for the former versus the latter. The metathetic synthesis presented herein offers economic as well as synthetic advantages compared to other reported procedures and yields greater than 90% are obtained.

Nanoparticle CdTe colloids have been employed as precursors for the spray deposition of CdTe thin films according to a one- or two-step method. CdTe films formed via a one-step approach were composed of the cubic CdTe phase as well as an oxide contaminant, $CdTe_2O_5$. A one-step film sprayed at 400 °C possessed smaller grains than a similar two-step film sprayed at 125 °C and annealed in forming gas as observed by AFM. While XPS analysis of a CdTe film sprayed at 400 °C showed no C contamination, an O signal, presumably from residual air during deposition, corresponded to a 4 wt % impurity level. Two-step CdTe films annealed in both forming gas and argon show similar phase development with cubic CdTe phase formation and increasing grain sizes with increasing annealing temperatures. Small amounts of Te metal are observed by XRD in films annealed at $T_{anneal} \leq 300$ °C in either argon or forming gas. Annealing at higher

temperatures ($T_{anneal} \geq 400$ °C) in either argon or forming gas leads to the gas-phase evolution of the Te metal owing to the substantial vapor pressure of Te at these temperatures. Two-step films possessed substantial C contamination as measured by XPS which may be due to the trapping of organic solvent and/or capping agent within the film bulk region during spray deposition at lower temperatures. $CdCl_2$ treatment of two-step CdTe films was found to promote crystalline phase development similar to that observed for nontreated films. AFM showed these $CdCl_2$-treated films possessed grains sizes from 300 to 1400 nm in diameter as a function of the concentration of the $CdCl_2$/methanol solution. Two-step prepared CdTe films processed at 400 °C and subjected to $CdCl_2$ treatment showed reduced impurity levels versus nontreated films as assayed by XPS with total impurity level ≤ 4 wt %.

A layer-by-layer growth mechanism has been proposed for the one-step spray deposition of nanoparticle precursors. Factors influencing this perspective include solvent flow rate, solvent heat capacity, carrier gas flow rate, carrier gas heat capacity, and sprayer head type. In-depth thermal analysis experiments are planned as a means to probe the mechanisms by which the methanol capping agent is evolved from the nanoparticle CdTe precursor during thin-film growth. It is expected that a more thorough understanding gained therein should provide the appropriate growth conditions whereby impurity contamination may be minimized with the maintenance of good film properties.

As a consequence of the evolution of nanoparticle science, revolutionary materials growth phenomenon such as colloidal self-organization[50] and solution–liquid–solid[51] processes have been established. Advanced organic/inorganic heterostructures such as nanoparticle–CdSe/semiconducting polymer light-emitting diodes exemplify the ability of the researcher to translate this nanotechnology into useful materials.[52] Likewise, we expect that the new technology of nanoparticle colloids as precursors to thin-film materials presented in this report will impact many polycrystalline device communities. In the near term, this approach seems directly transferable to members of the polycrystalline CdTe solar cell community. Extension of this approach to the spray deposition of other polycrystalline materials is under investigation.

(50) Murray, C. B.; Kagan, C. R.; Bawendi, M. G. *Science* **1995**, *270*, 1335–1338.
(51) Trentler, T. J.; Hickman, K. M.; Goel, S. C.; Viano, A. M.; Gibbons, P. C.; Buhro, W. E. *Science* **1995**, *270*, 1791–1794.
(52) Colvin, V. L.; Schlamp, M. C.; Alivasatos, A. P. *Nature* **1994**, *370*, 354–357.